ACS Synthetic Biology

pubs.acs.org/synthbio
Research Article

Development of a High Anthraquinone-Producing *Escherichia coli* Strain Using Malonyl-CoA Supply Pathway Engineering

Takatoshi Suematsu, Manami Takama, Itsuki Tomita, Shumpei Asamizu, Takahiro Bamba, and Tomohisa Hasunuma*

Cite This: *ACS Synth. Biol.* 2025, 14, 3957−3966
Read Online

ABSTRACT: Anthraquinones are valuable compounds that are traditionally used as natural pigments and have diverse pharmacological activities, including antimicrobial and anticancer effects. In this study, we aimed to enhance the production of 1,3,5-trihydroxyanthraquinone (AQ256) using *Escherichia coli* (*E. coli*) as a host. AQ256 is biosynthesized from eight malonyl-CoA molecules via the type II polyketide synthase pathway. However, previous studies have reported very low production levels of AQ256 in *E. coli* (approximately 2.5 mg/L), mainly because of limited malonyl-CoA availability. To address this, we introduced a heterologous malonate assimilation pathway and reinforced the endogenous malonyl-CoA biosynthesis pathway. An *E. coli* strain harboring AQ256 biosynthetic genes from *Photorhabdus laumondii* TTO1 produced only 1.3 mg/L AQ256. Upon introducing the malonate assimilation pathway and cultivating in malonate-supplemented Luria−Bertani medium, production increased to 3.8 mg/L. Further enhancement of the endogenous malonyl-CoA supply through the coexpression of pantothenate kinase and acetyl-CoA carboxylase resulted in strain AQ-04, which produced 12.3 mg/L AQ256. Optimization of cultivation conditions enabled AQ-04 to achieve 23.9 mg/L AQ256, a 9.6-fold increase compared to previous studies. Our results demonstrate that the combination of introducing a malonate assimilation pathway and enhancing native malonyl-CoA supply is a highly effective strategy for increasing malonyl-CoA availability. This approach is promising for the biosynthesis of a wide range of malonyl-CoA-derived compounds.

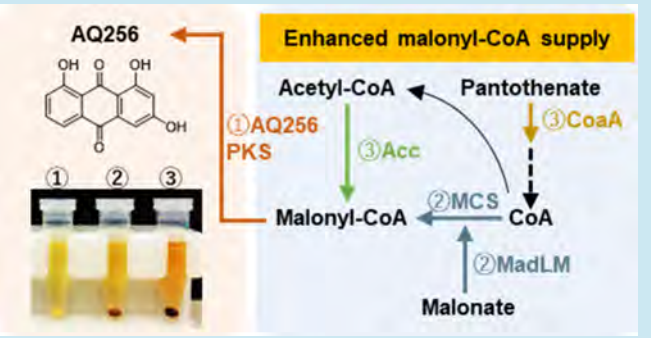

KEYWORDS: *Escherichia coli, anthraquinone, 1,3,5-trihydroxyanthraquinone (AQ256), metabolic engineering, malonyl-CoA, type II polyketide synthase*

INTRODUCTION

Anthraquinones are a group of compounds with a basic 9,10-anthracenedione skeleton consisting of three tandemly fused hexacyclic ring systems with two carbonyl groups (Figure 1A). The backbone contains a π-conjugated system, allowing it to absorb visible light, and has therefore been historically used as a dye.[1,2] In addition, anthraquinones exhibit diverse pharmacological activities owing to their quinone structure, which can oxidize the substrate, leading to hydrogen (−H) substitution with various functional groups or sugars.[3−5] Consequently, anthraquinones exhibit bioactivity as laxatives, antibacterials, antifungals, and anticancer agents.[6,7]

Anthraquinones are secondary metabolites found in microorganisms, insects, and plants and are generally synthesized via the action of polyketide synthase (PKS).[6,8−10] Some anthraquinones in plants are biosynthesized from precursors derived from shikimate or terpenoid biosynthetic pathways.[11] PKS enzymes are classified into three types based on their structural and mechanistic properties: I, II, and III. Anthraquinones are produced through complex reaction mechanisms mediated by type II PKS composed of monofunctional enzyme complexes.[12] In the type II PKS reaction, polyketide chains of varying lengths are generated, depending on the number of starter and extender units, by the action of a ketosynthase (KS)/chain length factor (CLF), a minimal unit in type II PKS. Subsequently, aromatase/cyclase, dehydratases, and other dedicated tailoring enzymes generate aromatic scaffolds.[10,13]

The large-scale production of various anthraquinones remains a challenge because of the high cost and time-consuming nature of plant and insect extraction.[14] Microbial production is also complicated by the complexity of genetic

Received: May 15, 2025
Revised: August 17, 2025
Accepted: September 8, 2025
Published: September 16, 2025

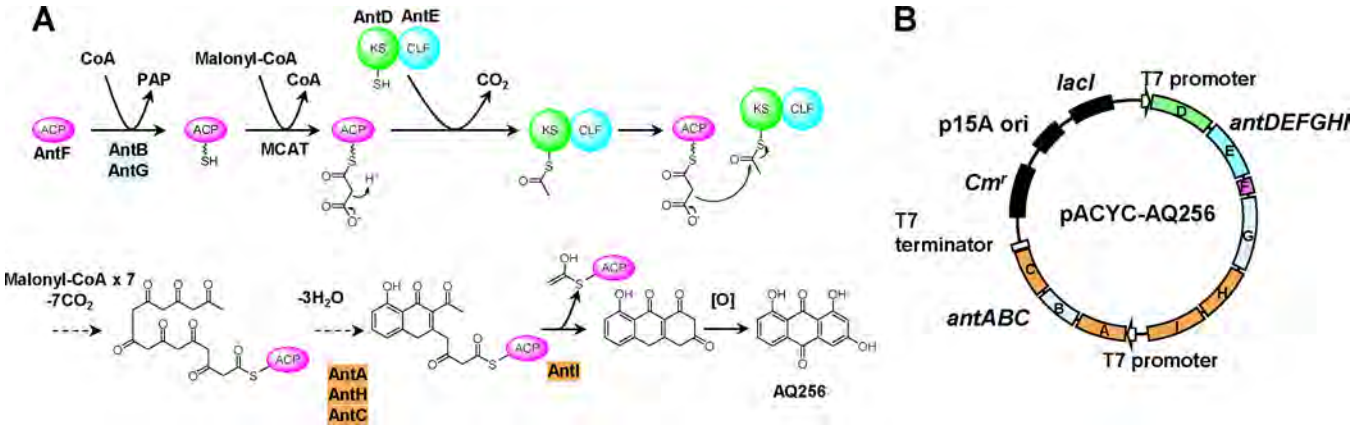

Figure 1. (A) Biosynthetic pathway of AQ256 and (B) the plasmid for heterologous expression of the AQ256 gene cluster in *E. coli* AQ256 utilizes eight malonyl-CoA as a substrate, involving nine AQ256 biosynthetic enzymes (AntA–I) from *P. laumondii* TTO1 and endogenous *E. coli* enzymes functioning as MCAT. Since the original *ant* biosynthetic genes are organized into two operons (*antABC* and *antDEFGHI*), a plasmid was constructed to independently express each operon under separate T7 promoters. Abbreviations: CoA, coenzyme A; PAP, 3′-phosphoadenosine 5′-phosphate; AntA, ketoreductase; AntB, phosphopantetheinyl transferase; AntC, cyclase; AntDE, ketosynthase $\alpha\beta$ heterodimer; AntF, acyl carrier protein; AntG, coenzyme A ligase; AntH, aromatase; AntI, hydrolase; MCAT, malonyl-CoA-acyl carrier protein transacylase.

modifications and lack of established large-scale fermentation techniques.[15]

Recently, metabolic engineering and synthetic biology approaches have been explored to develop microbial strains with enhanced anthraquinone production. For example, the production of flavokermesic acid,[16] dehydrorabelomycin,[17,18] and 1,3,5-trihydroxyanthraquinone (AQ256)[19] has been reported in *Escherichia coli* (*E. coli*). However, the low production yields remain a major challenge for these anthraquinones.

This study aimed to achieve high-level heterologous production of anthraquinones using metabolic engineering, focusing on the development of an *E. coli* strain optimized for AQ256 production. *E. coli* is a well-characterized prokaryotic model organism with extensive genetic and metabolic information.[20] Owing to its ease of genetic manipulation and rapid growth, *E. coli* has been widely used as a production host for valuable compounds,[17,21] including type II polyketide products, via the heterologous expression of biosynthetic gene clusters, making it a promising candidate for anthraquinone biosynthesis. AQ256 is an aromatic polyketide synthesized via type II PKS, and its biosynthetic pathway is well-characterized.[22] Moreover, the culture medium takes on a color ranging from red to brown, which allows easy monitoring of production during the cultivation process.

AQ256 was biosynthesized using eight malonyl-CoA molecules as precursors by expressing nine *ant* genes (*antA–I*) derived from *Photorhabdus laumondii* (*P. laumondii*) TTO1 in *E. coli* (Figure 1A).[19] Malonyl-CoA is essential for fatty acid biosynthesis; however, its accumulation is limited and the production capacity for nonessential metabolites is restricted.[23,24] In *E. coli*, a high malonyl-CoA supply can be achieved via two major strategies: strengthening endogenous biosynthetic pathways[25−28] and introducing heterologous metabolic pathways for malonyl-CoA synthesis from malonate.[29−31] Strengthening the endogenous malonyl-CoA biosynthetic pathway via acetyl-CoA carboxylase gene expression contributes to enhanced anthraquinone production.[16] In *E. coli*, malonyl-CoA is synthesized from acetyl-CoA via a reaction catalyzed by acetyl-CoA carboxylase (Acc). On the other hand, heterologous malonyl-CoA supply pathways based on *matB*/*matC* from *Rhizobium trifolii* (MatB: malonyl-CoA synthetase; MatC: malonate transporter) have been widely investigated for enhancing the biosynthesis of value-added metabolites such as flavonoids and hydroxy acids.[29,31] However, the application of these pathways to anthraquinone biosynthesis remains limited, and their integration with endogenous malonyl-CoA biosynthetic pathway enhancement has not been thoroughly explored.

In this study, we first evaluated the effect of introducing an exogenous malonate assimilation pathway into *E. coli* on the production of AQ256. Additionally, strains with enhanced endogenous malonyl-CoA biosynthesis were constructed to investigate the combined effects of the two approaches. The AQ256 production levels of these engineered strains, along with the intracellular CoA-related metabolite pools, were evaluated. Finally, cultivation conditions were optimized by adjusting medium composition and initial cell density to maximize AQ256 production.

RESULTS

Heterologous Production of AQ256 by *E. coli* BL21 (DE3). AQ256 can be produced in *E. coli* by expressing nine *ant* genes (*antA–I*) derived from the *P. laumondii* TTO1 strain.[19] In the AQ256 biosynthesis pathway, the apo-form acyl carrier protein (ACP; AntF), which lacks the 4′-phosphopantetheine prosthetic group and is catalytically inactive, is activated by phosphopantetheinyl transferase (AntB) and coenzyme A ligase (AntG). These enzymes consume coenzyme A (CoA) and convert apo-ACP into the holo-form, which carries the 4′-phosphopantetheine moiety and serves as the active carrier of acyl intermediates (Figure 1A). Subsequently, malonyl-CoA is loaded onto the ACP using malonyl-CoA-acyl carrier protein transacylase (MCAT). This catalytic reaction is presumably mediated by endogenous *E. coli* enzymes functioning as MCAT.[19] The malonyl-ACP then undergoes polyketide chain elongation catalyzed by the ketosynthase $\alpha\beta$ heterodimer (AntDE), ultimately leading to the decarboxylative Claisen condensation of eight malonyl-CoA molecules to form an octaketide chain. The resulting octaketide chain is cyclized by ketoreductase (AntA), aromatase (AntH), and cyclase (AntC). Furthermore, AntI,

https://doi.org/10.1021/acssynbio.5c00354
ACS Synth. Biol. 2025, 14, 3957−3966

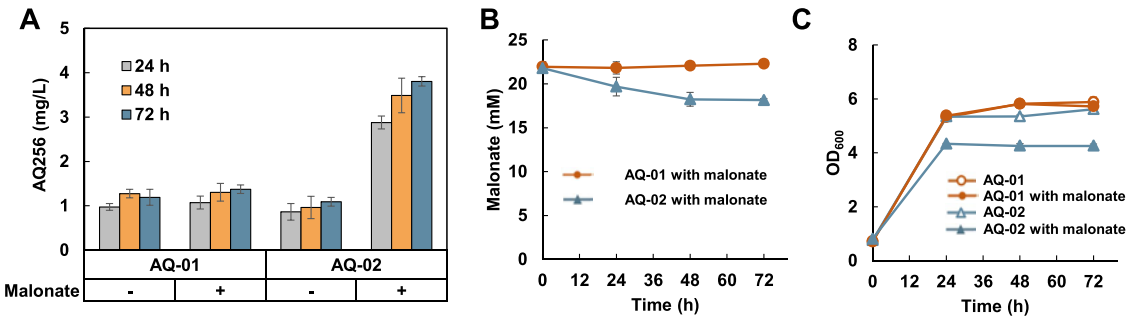

Figure 2. Effect of the heterologous malonate assimilation pathway on AQ256 production in *E. coli* (A) AQ256 production by AQ-01 and AQ-02 with or without malonate supplementation. A "+" indicates the addition of 22 mM malonate in the medium. The AQ-01 strain contains the AQ256 biosynthetic genes, while the AQ-02 strain contains both the AQ256 biosynthetic genes and the malonate assimilation pathway. Time course of (B) malonate consumption and (C) growth of AQ-01 and AQ-02. Results are presented as the mean ± standard deviation of three biologically independent experiments.

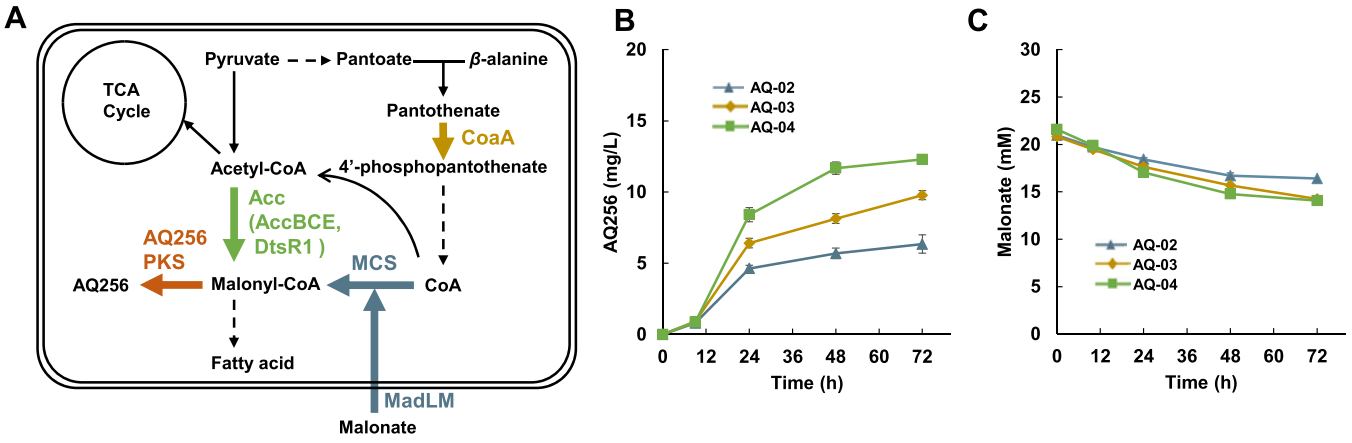

Figure 3. Effect of the enhanced endogenous malonyl-CoA biosynthesis pathway on AQ256 production in *E. coli* (A) Endogenous malonyl-CoA biosynthesis pathway of *E. coli*. Solid arrows indicate single reaction steps, and the dashed arrows indicate multiple enzymatic steps. The metabolic reactions enhanced in this study are indicated by colored arrows (red, blue, yellow, and green). Abbreviations: MadLM, malonate transporter from *M. rubra*; MCS, malonyl-CoA synthetase from *B. japonicum*; Acc, acetyl-CoA carboxylase from *C. glutamicum*; CoaA, pantothenate kinase from *P. putida*. Time course of (B) AQ256 production and (C) malonate consumption of AQ-02, AQ-03, and AQ-04 strains. Strains AQ-03 and AQ-04 were constructed by overexpressing *Pp-coaA* and both *Pp-coaA* and *Cg-acc*, respectively, in the AQ-02 host strain. Data represent the mean ± standard deviation from three independent biological experiments.

an unusual lyase, cleaves the acetyl unit while promoting cyclization to form a cyclized heptaketide scaffold and the consequent release of acetyl-ACP. The released heptaketide product is spontaneously oxidized to yield AQ256.[19,22]

In this study, *ant* genes were divided into two operons (*antA*−*C* and *antD*−*I*) and ligated under the T7 promoter to produce the pACYC-AQ256 plasmid (Figure 1B). The *E. coli* BL21 (DE3) strain harboring pACYC-AQ256 was designated AQ-01. AQ-01 was cultivated in Luria−Bertani (LB) medium, and the AQ256 production level was evaluated. As a result, AQ256 production by AQ-01 reached 1.3 ± 0.1 mg/L at 48 h of cultivation (Figure 2A).

Malonyl-CoA Supply Enhancement via Exogenous Malonate Assimilation Pathway Introduction. Since AQ256 biosynthesis requires eight molecules of malonyl-CoA (Figure 1A), we hypothesized that introducing the malonate assimilation pathway may enhance the malonyl-CoA supply and, consequently, AQ256 production. To convert malonate into malonyl-CoA, a Na^+-dependent malonate transporter encoded by the malonate transporter gene (*madLM*) from *Malonomonas rubra* (*M. rubra*) and the malonyl-CoA synthetase gene (*mcs*) from *Bradyrhizobium japonicum* (*B. japonicum*) was expressed in *E. coli*. The expression of *madLM* and *mcs* in *E. coli* has been reported to increase the (2S)-naringenin production, which uses malonyl-CoA as a precursor.[30] Here, plasmids harboring *madLM* and *mcs* with the T7 promoter were introduced into AQ-01 to construct strain AQ-02.

The effect of malonate supplementation (22 mM) in LB medium on AQ256 production was evaluated in the AQ-01 and AQ-02 strains. No significant increase in AQ256 production was observed upon malonate supplementation of AQ-01 (Figure 2A). In contrast, in AQ-02, although AQ256 production was 1.1 ± 0.1 mg/L without malonate supplementation, increased to 2.9 ± 0.1 mg/L with addition of malonate, representing a 2.7-fold increase. Moreover, AQ256 production in AQ-02 did not increase after 24 h in the absence of malonate, whereas it continued to increase in the presence of malonate, reaching 3.8 ± 0.1 mg/L at 72 h. AQ-02 consumed 3.6 mM malonate at 72 h, whereas no significant consumption was observed in AQ-01 (Figure 2B). Malonate supplementation showed no effect on cell growth (OD_{600}: 5.7 ± 0.1) in AQ-01 (Figure 2C); in AQ-02, OD_{600} only reached to 4.3 ± 0.1 upon malonate supplementation at 72 h. These results indicate that although malonate supplementation reduced the cell density of AQ-02 cells,

https://doi.org/10.1021/acssynbio.5c00354
ACS Synth. Biol. 2025, 14, 3957−3966

AQ256 production per cell increased. AQ256 production was enhanced by introducing the malonate assimilation pathway and malonate supplementation.

To examine whether the decrease in cell density caused by malonate supplementation could be alleviated, the AQ-02 strain was cultured under a reduced malonate concentration (7.3 mM). As a result, after 72 h of cultivation, cell growth remained similarly suppressed as under the 22 mM condition (OD_{600}: 4.3 ± 0.1) (Figure S1A), and AQ256 production decreased to 2.7 ± 0.1 mg/L (Figure S1B). Based on these results, subsequent experiments in this study were conducted using 22 mM malonate as the experimental condition.

***Pp-coaA* and *Cg-acc* Expression to Strengthen the Endogenous Malonyl-CoA Production Pathway.** In this study, the effects of enhanced CoA synthesis and acetyl-CoA carboxylation on AQ256 production were investigated (Figure 3A). Pantothenate kinase (CoaA), which phosphorylates pantothenate, is the initial step of CoA biosynthesis to produce 4′-phosphopantothenate. The pantothenate kinase gene (*Pp-coaA*) from *Pseudomonas putida* (*P. putida*) was selected for overexpression because, unlike CoaA from *E. coli*, *Pp*-CoaA is not subject to feedback inhibition by CoA, acetyl-CoA, or malonyl-CoA.[33] *Pp-coaA* overexpression enhances the supply of CoA and acetyl-CoA in *E. coli*.[28,32] Acetyl-CoA carboxylase catalyzes the ATP-dependent conversion of acetyl-CoA to malonyl-CoA. The *acc* gene from *Corynebacterium glutamicum* (*C. glutamicum*) (*Cg-acc*), which is evolutionarily distinct from the four-subunit Acc complex of *E. coli*, encodes a three-subunit enzyme complex that exhibits higher activity at low temperatures (approximately 23 °C) compared to Acc from *E. coli*.[27,33] Therefore, it is expected to efficiently convert acetyl-CoA to malonyl-CoA even under low-temperature conditions, which are generally required for the expression of polyketide synthase in *E. coli*.

First, the AQ-03 strain was constructed by overexpressing *Pp-coaA* in the AQ-02 strain, and the AQ-04 strain was constructed by overexpressing both *Pp-coaA* and *Cg-acc* (*accBC*, *accE*, and *dtsR1* genes). The strains were cultivated for 72 h in LB medium supplemented with malonate. As a result, AQ256 production in AQ-03 and AQ-04 reached 9.8 ± 0.3 and 12.3 ± 0.2 mg/L, respectively, representing 1.5-fold and 1.9-fold increases compared to AQ-02 (Figure 3B). Additionally, malonate consumption in the culture medium was 4.6 mM in AQ-02, 6.6 mM in AQ-03, and 7.5 mM in AQ-04 (Figure 3C). These results demonstrate that *Pp-coaA* and *Cg-acc* overexpression further enhanced malonate uptake and AQ256 production in *E. coli* strains harboring the malonate assimilation pathway.

To clarify the effects of enhancing only the endogenous pathway, the AQ-03 and AQ-04 strains were also cultivated in LB medium without malonate supplementation. After 72 h of cultivation, AQ256 production reached 1.5 ± 0.0 mg/L in AQ-03 and 3.5 ± 0.3 mg/L in AQ-04, both of which were lower than the corresponding values under malonate-supplemented conditions (Figure S2 and Figure 3B). These results clearly demonstrate that the improvement in AQ256 production was achieved through the synergistic effect of introducing a heterologous malonate assimilation pathway and enhancing the endogenous malonyl-CoA biosynthesis pathway.

Measurement of Intracellular CoA Compounds in Malonyl-CoA Supply-Enhanced Strains. To investigate the effect of gene overexpression on the intracellular pools of CoA-related compounds, we analyzed the accumulation of CoA-related compounds (CoA, acetyl-CoA, and malonyl-CoA) in the engineered cells. Strains AQ-01−AQ-04 were cultured in LB medium supplemented with 22 mM malonate. Intracellular metabolites were analyzed using liquid chromatography-tandem mass spectrometry (LC-MS/MS) to measure the concentrations of CoA-related compounds. Metabolic analysis revealed that the total concentration of CoA-related compounds in all strains was highest at 9 h of cultivation and then decreased over time (Figure 4). As expected, at 9 h of cultivation, the malonyl-CoA concentration in strain AQ-02 (0.87 nmol/mg-DCW) was 6.2-fold higher than that in AQ-01 (0.14 nmol/mg-DCW). However, after 24 h of cultivation, no significant differences in malonyl-CoA accumulation were observed between the AQ-01 and AQ-02 cells. In strains AQ-03 and AQ-04, the endogenous malonyl-CoA supply pathway was enhanced in addition to the introduction of the malonate assimilation pathway. At 9 h of cultivation, the CoA accumulation levels in AQ-03 and AQ-04 were 1.4 and 1.1 nmol/mg-DCW and in acetyl-CoA were 1.5 and 2.0 nmol/mg-DCW, respectively. These values were higher than those observed in AQ-02 (CoA: 0.6 nmol/mg-DCW, acetyl-CoA: 1.0 nmol/mg-DCW). Despite the higher AQ256 production observed in AQ-03 and AQ-04 than in AQ-02 (Figure 3B), the accumulation of malonyl-CoA remained similar among these strains throughout the cultivation period. This result suggests that malonyl-CoA was rapidly consumed in strains AQ-02, AQ-03, and AQ-04. However, considering that the best-performing strain, AQ-04, consumed approximately 7.5 mM malonate while producing only 12.3 ± 0.2 mg/L AQ256 (Figure 3C), it is likely that a substantial portion of the generated malonyl-CoA was diverted to competing endogenous pathways, such as fatty acid biosynthesis.

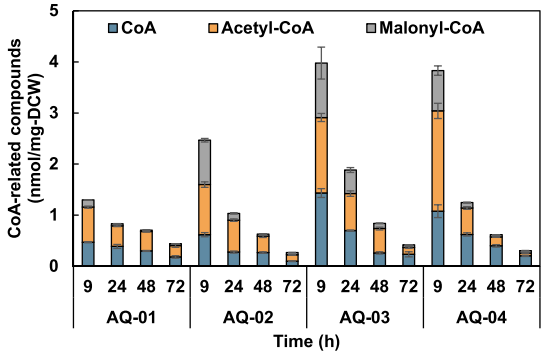

Figure 4. Intracellular concentration of CoA-related compounds in the engineered strains. The vertical axis represents the total concentration of CoA-related metabolites, including CoA, acetyl-CoA, and malonyl-CoA. Results are expressed as means ± standard deviation of three independent biological experiments.

Optimization of Medium Composition: Effects of Glucose and LB Medium Components. AQ256 production was conducted in LB medium without the addition of carbon sources other than malonate. Metabolite analysis revealed a rapid decrease in the levels of CoA, acetyl-CoA, and malonyl-CoA after 24 h of cultivation (Figure 4). To further enhance the supply of CoA derivatives, we examined the effects of glucose supplementation or additional yeast extract (a mixture of vitamins and amino acids) to LB medium supplemented with malonate on the AQ256 production. The AQ-04 strain,

https://doi.org/10.1021/acssynbio.5c00354
ACS Synth. Biol. 2025, 14, 3957−3966

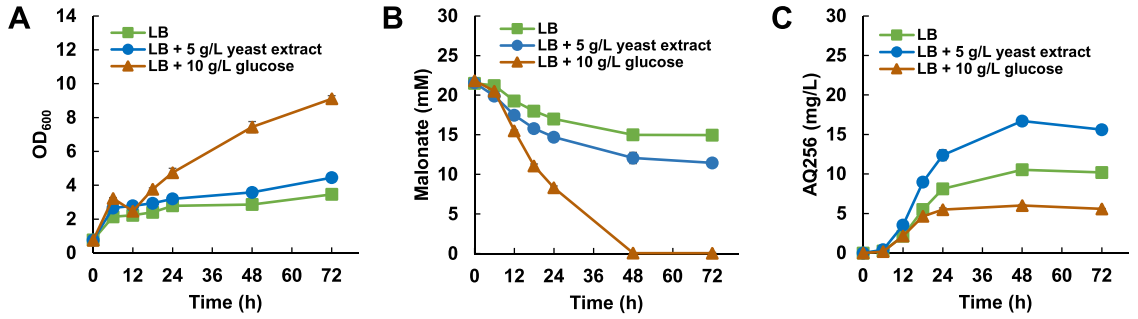

Figure 5. Effect of glucose or yeast extract supplementation on AQ256 production by strain AQ-04 in LB medium containing 22 mM malonate. Time course of (A) growth, (B) malonate consumption, and (C) AQ256 production by AQ-04 in three different medium conditions. Data represent the mean ± standard deviation of three independent biological experiments.

which exhibited the highest AQ256 production, was used to evaluate these effects.

As shown in Figure 5A, the addition of glucose to the medium resulted in a 2.6-fold increase in OD_{600} at 72 h of cultivation (OD_{600} = 9.1 ± 0.2) compared to cultures without glucose. Notably, glucose supplementation promoted malonate consumption, leading to complete malonate depletion after 48 h of culture (Figure 5B). Glucose was almost completely consumed after 48 h (Figure S3). However, AQ256 production was only 5.6 ± 0.1 mg/L at 72 h, which was notably lower than the titer without adding glucose (Figure 5C). Next, the addition of 5 g/L yeast extract slightly increased OD_{600} at 72 h (OD_{600} = 4.5 ± 0.1) compared to control conditions (Figure 5A). Malonate consumption also improved marginally, with 10.1 mM being consumed within 72 h (Figure 5B). Furthermore, AQ256 production at 72 h reached 15.6 ± 0.2 mg/L, representing a 1.5-fold increase compared to cultures without additional yeast extract (Figure 5C). Although additional yeast extract enhanced AQ256 production, the increase from 24 h (12.4 ± 0.7 mg/L) to 72 h (15.6 ± 0.2 mg/L) was only 26%, indicating that AQ256 production did not significantly improve production in the stationary phase.

To further investigate how medium composition affects AQ256 biosynthesis, we also evaluated AQ256 production in the AQ-04 strain using M9 medium containing 10 g/L glucose and 22 mM malonate as the carbon source. After 72 h of cultivation in M9 medium, AQ-04 exhibited an OD_{600} of 1.2 ± 0.1 and produced 1.4 ± 0.0 mg/L AQ256 (Figure S4). These values were lower than those obtained when AQ-04 was cultivated in LB medium. Compared to minimal M9 medium conditions, the nutrient-rich LB medium provides a more favorable environment for both cellular growth and efficient AQ256 production.

Effect of Initial Cell Density on AQ256 Production. Our experiments demonstrated that most AQ256 production occurred within the first 24 h of cultivation. Analysis of CoA derivatives showed a rapid increase in the intracellular CoA concentration at the start of cultivation, followed by a sharp decline, which is consistent with a previous study on fatty acid biosynthesis.[27] Therefore, to increase the number of cells involved in the production for AQ256 up to 24 h of incubation, the effects on the initial cell density (OD_{600}) were investigated.

The AQ-04 strain was cultured in LB medium supplemented with 5 g/L yeast extract, and the cells were harvested 6 h after IPTG induction. Harvested cells were inoculated into fresh medium (LB + 5 g/L yeast extract + 22 mM malonate) at OD_{600} values of 0.5, 2.3, and 4.4. The results showed that after 72 h of cultivation, both OD_{600} and malonate consumption increased proportionally with the initial cell density. At an initial OD_{600} of 4.4, the final OD_{600} reached 7.3 ± 0.1, and 12.8 mM malonate was consumed (Figure 6A,B). Along with the

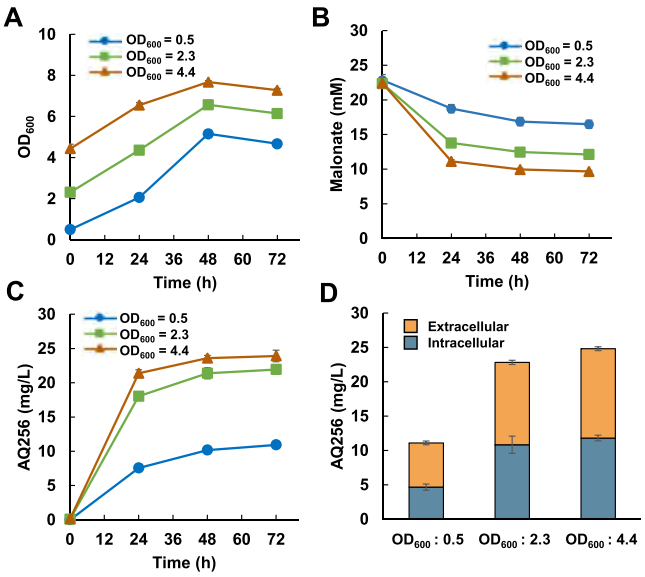

Figure 6. Effects of initial cell density on AQ256 production in the AQ-04 strain. Time course of (A) growth, (B) malonate consumption, and (C) AQ256 production by AQ-04 at different initial OD_{600}. (D) Ratio of intracellular and extracellular AQ256 levels after 72 h of cultivation. Results are presented as means ± standard deviation of three independent biological experiments.

higher initial cell densities, AQ256 production increased, reaching 23.9 ± 0.9 mg/L at an initial OD_{600} of 4.4, which was 2.2-fold higher than at an initial OD_{600} of 0.5 and 9.6-fold higher than the previous study by Cummings et al. (2.5 mg/L)[19] (Figure 6C).

During AQ-04 cultivation, both the cells and the culture medium exhibited a reddish-brown coloration. Therefore, we measured AQ256 concentration in both the intracellular and extracellular fractions after 72 h of cultivation (Figure 6D). The results indicated that the ratio of intracellular to extracellular AQ256 was approximately 46%:54%, regardless of the initial cell density, suggesting that nearly half of the AQ256 accumulated inside the cells. These findings indicated that increasing the initial cell density enhanced early cell growth and malonate uptake, thereby improving AQ256 production efficiency.

https://doi.org/10.1021/acssynbio.5c00354
ACS Synth. Biol. 2025, 14, 3957−3966

Finally, to investigate whether metabolic redirection in the AQ-04 strain through inhibition of fatty acid synthesis could enhance AQ256 production, we conducted cultivation under the condition that yielded the highest AQ256 production (initial OD_{600} = 4.4) with the addition of 50 μM cerulenin, a known inhibitor of fatty acid synthase.[34] However, after 72 h of cultivation, the AQ256 production decreased (4.6 ± 0.2 mg/L) compared to that without cerulenin supplementation (Figure S5). Although the reason for the decreased AQ256 production upon cerulenin addition remains unclear, Omura suggested that cerulenin may inhibit the reactions of PKS.[34]

DISCUSSION

Previous studies have primarily focused on enhancing the endogenous malonyl-CoA biosynthetic pathways to improve anthraquinone production. However, the effects of introducing an exogenous malonate assimilation pathway on anthraquinone production have not yet been investigated. Therefore, in this study, we first investigated the effect of strengthening the exogenous malonyl-CoA supply by introducing a malonate assimilation pathway on the production of AQ256. The results showed that the AQ-02 strain carrying the malonate assimilation pathway exhibited a 2.9-fold increase in AQ256 production compared to the AQ-01 strain, which lacked the malonate assimilation pathway (Figure 2A). In contrast, a previous study reported that overexpression of *madLM* and *mcs* in *E. coli* led to a 6.8-fold increase in (2S)-naringenin production.[30] This difference in the rate of increase in production may be attributable to the different numbers of malonyl-CoA molecules required: the biosynthesis of (2S)-naringenin requires three molecules of malonyl-CoA, whereas AQ256 production requires eight. Therefore, in the present study, we developed the AQ-04 strain, in which the endogenous malonyl-CoA supply pathway was also enhanced, to further increase malonyl-CoA availability. The AQ-04 strain showed a 1.9-fold increase in AQ256 production compared to the AQ-02 strain (Figure 3B). These results indicate that enhancement of malonyl-CoA supply is effective in improving AQ256 production in *E. coli*. However, even in the AQ-04 strain, the intracellular level of CoA-related compounds, including malonyl-CoA, rapidly decreased after 24 h of cultivation (Figure 4). In future studies, time course monitoring of the levels of overexpressed *Pp*-CoaA and intracellular *Cg*-Acc in the AQ-04 strain using proteomic analysis may help to clarify the underlying cause. To the best of our knowledge, this study is the first successful demonstration that the integration of exogenous malonate assimilation and endogenous malonyl-CoA biosynthetic pathway enhancement can synergistically increase the production of a malonyl-CoA-derived compound.

Despite the introduction of the malonate assimilation pathway, 14.5 mM malonate remained unconsumed in the culture medium of AQ-04 even after 72 h of cultivation in LB medium supplemented with 22 mM malonate (Figure 3C). The limited uptake of malonate under glucose-free conditions suggests that the conversion of malonate to malonyl-CoA is the rate-limiting step in the malonate assimilation pathway. This reaction is catalyzed by malonyl-CoA synthetase (MCS), an ATP-dependent enzyme.[30,35] Intracellular ATP levels were measured, which showed a gradual decrease after 9 h of cultivation (Figure S6), potentially limiting the activity of MCS and subsequently reducing the efficiency of malonate utilization. Consequently, the slow conversion of intracellular malonate to malonyl-CoA likely leads to malonate accumulation inside the cells, which in turn reduces the driving force for further malonate uptake from the medium. In contrast, when glucose was added to the medium to enhance CoA biosynthesis, the AQ-04 strain completely consumed all 22 mM malonate (Figure 5B). This suggests that glucose supplementation provided sufficient ATP to support MCS activity. Unexpectedly, the addition of glucose decreased AQ256 production (Figure 5C). Additionally, the total intracellular concentration of CoA-related compounds was lower after 9 h of cultivation under glucose-supplemented conditions than that under glucose-free conditions (Figure S7). These results suggest that glucose supplementation activated the TCA cycle, leading to the preferential utilization of acetyl-CoA for bacterial growth, whereas malonyl-CoA was diverted toward fatty acid biosynthesis required for cell proliferation. Indeed, under glucose-supplemented conditions, bacterial growth continued beyond 18 h of culture (Figure 5A). Given that glucose is an inexpensive carbon source, the development of engineering strategies to enhance AQ256 production from glucose remains an important challenge for future research.

An interesting phenomenon observed under glucose supplementation was the absence of reddish-brown coloration in the supernatant, which is typically associated with AQ256 production. A comparative analysis of intracellular and extracellular AQ256 levels revealed that under glucose-supplemented conditions, a larger proportion of AQ256 accumulated intracellularly (Figure S8). Although the exact reason for this remains unclear, the substrate specificity of various *E. coli* transporters can change depending on the environmental conditions.[36] Furthermore, small organic acids such as acetate generated by glucose metabolism are preferentially exported over AQ256.

In addition to glucose supplementation, we also examined the effects of yeast extract supplementation. The addition of 5 g/L yeast extract to LB medium resulted in an increase in AQ256 production (Figure 5C). This improvement may be attributed to the presence of CoA biosynthesis precursors such as β-alanine and pantothenic acid in yeast extract.[37,38] These compounds may synergistically enhance the CoA supply in combination with the expression of *Pp-coaA* (Figure 3A).

To further enhance AQ256 production, improving the enzymatic activity of the AQ256 PKS is also critical. Yang et al. reported that the coexpression of polyketide chain-synthesizing enzymes (*antD, antE, antF, antB,* and *antG*; Figure 1A) and heterogeneous cyclases (*zhuI* and *zhuJ* from *Streptomyces* sp. R1128) in *E. coli* BAP1 resulted in the production of 88.0 mg/L flavokermesic acid and oktaketide.[16] These findings suggest that in AQ256 biosynthesis, the enzymatic reactions for cyclization and subsequent acetyl-ACP cleavage (catalyzed by *antA, antH, antC,* and *antI* gene products; Figure 1A) might be the rate-limiting steps. Future studies should focus on optimizing the expression levels of these enzymes and/or enhancing their catalytic activities through protein engineering to improve AQ256 production.

In addition to enzymatic activity, limitations in the expression levels and stability of AntA−I proteins may also influence the efficiency of AQ256 biosynthesis, particularly during the stationary phase. Therefore, relative quantification of AntA−I protein expression at different cultivation time points using proteomic approaches may help clarify whether

https://doi.org/10.1021/acssynbio.5c00354
ACS Synth. Biol. 2025, 14, 3957−3966

the reduced AQ256 production observed at later stages of cultivation is attributable to insufficient protein abundance.

Moreover, in the initially designed strain, the transfer of malonyl-CoA to ACP relied on the endogenous MCAT from *E. coli*. Since the compatibility between ACP and acyltransferase is known to affect the efficiency of polyketide biosynthesis, this step was considered a potential rate-limiting factor. Accordingly, we introduced the MCAT gene derived from *P. laumondii* TTO1 (*Pl-mcat*) into the AQ-04 strain. Indeed, introduction of *Pl-mcat* into the AQ-04 strain increased AQ256 production by 1.3-fold, reaching 16.3 ± 1.8 mg/L (Figure S9). This improvement may be attributed either to elevated MCAT expression or to the *P. laumondii*-derived MCAT being more suitable for transferring malonyl-CoA to ACP than the endogenous *E. coli* MCAT.

In this study, we established a method for high-yield production of AQ256 in *E. coli*. This system has the potential to be applied for the high-yield production of other valuable anthraquinone derivatives by incorporating other modification enzymes into the AQ256 biosynthetic system. The malonyl-CoA enhancement strategy established in this study may also be applicable to broader biosynthesis of polyketides, including other anthraquinones.

METHODS

Strains and Media. The *E. coli* strains used in this study are listed in Table S1. The *E. coli* DH5α strain was used for plasmid construction and amplification. *E. coli* strains were routinely cultivated in LB medium (10 g/L tryptone, 5 g/L yeast extract, and 5 g/L NaCl; Nacalai Tesque, Kyoto, Japan) with appropriate antibiotics (50 μg/mL chloramphenicol, 100 μg/mL kanamycin, 50 μg/mL spectinomycin, and 100 μg/mL ampicillin) at 37 °C with shaking at 200 rpm.

Plasmid Construction. The plasmids and polymerase chain reaction (PCR) primers used in this study are listed in Tables S2 and S3. All synthetic genes were synthesized using GeneArt (Thermo Fisher Scientific, Waltham, MA, USA). All plasmids were constructed using an In-Fusion HD cloning kit (Takara Bio, Mountain View, CA, USA) according to the manufacturer's instructions.

The pACYC-AQ256 plasmid was constructed as follows: AQ256 biosynthetic genes from the *P. laumondii* subsp. *laumondii* TTO1 strain (MIBiG no. BGC0000196) was synthesized in four fragments (Figure S10). The DNA fragment encoding *antA*−*antC* genes was amplified from the synthetic gene by PCR using AQ256_fragment4_Fw_NdeI and AQ256_fragment4_Rv_Xho primers. The *antA*−*antC* fragment was inserted into the pACYCDuet-1 vector, which was double-digested with *Nde*I and *Xho*I to generate the pACYC-AntA-C plasmid. The DNA fragment encoding *antD*−*antI* genes was amplified from the three synthetic gene fragments using AQ256_fragment1_Fw_NcoI, AQ256_fragment1_Rv, AQ256_fragment2_Fw, AQ256_fragment2_Rv, AQ256_fragment3_Fw, and AQ256_fragment3_Rv_*Pst*I primers. The *antD*−*antI* fragments were inserted into pACYC-AntA-C, which was double-digested with *Nco*I and *Pst*I, to generate the pACYC-AQ256 plasmid.

The pACYC-AQ256-MCAT plasmid was constructed as follows: The DNA fragment encoding the malonyl-CoA acyl carrier protein transacylase (MCAT) gene from *P. laumondii* TTO1 was amplified from the synthetic gene using the pACYC-MCAT-Fw and pACYC-MCAT Rv primers. The resulting MCAT fragment was inserted into pACYC-AQ256, which had been double-digested with *Xho*I and *Avr*II, to generate pACYC-AQ256-MCAT.

The pMW219-MadLM plasmid was constructed as follows: The DNA fragment encoding the *madLM* gene from *M. rubra* was amplified from the synthetic gene using madLM_Fw and madLM_Rv primers. The DNA fragments encoding the T7 promoter and T7 terminator were amplified from the pETDuet-1 vector using madLM_pro_Fw, madLM_pro_Rv, madLM_ter_Fw, and madLM_ter_Rv. The *madLM*, T7 promoter, and T7 terminator fragments were inserted into pMW219 DNA (Nippon Gene, Tokyo, Japan), which was double-digested with *Eco*RI and *Bam*HI to generate the pMW219-MadLM plasmid.

The pET-mcs plasmid was constructed as follows: The *mcs* gene from *B. japonicum* was codon-optimized for *E. coli* and synthesized. The DNA fragment encoding the *mcs* gene was amplified from the synthetic gene using the pETDuet_MCS_Fw and pETDuet_MCS_Rv primers. The *mcs* fragment was inserted into pETDuet-1, which was double-digested with *Nco*I and *Bam*HI to generate the pET-mcs plasmid.

The pCDF-CoaA plasmid was constructed as follows: The CoaA gene from *P. putida* was codon-optimized for *E. coli* and synthesized. The DNA fragment encoding *coaA* was amplified from the synthetic gene using the pCDF-coaA Fw and pCDF-coaA Rv primers. The *coaA* fragment was inserted into pCDFDuet-1, which was double-digested with *Nde*I and *Avr*II to generate pCDF-CoaA.

The plasmid pCDF-Acc-CoaA was constructed as follows: The DNA fragments encoding *accBC, accE,* and *dtsR1* genes were amplified from the *C. glutamicum* ATCC 13032 genome using the pCDF-accBC Fw, pCDF-accBC Rv, pCDF-accE Fw, pCDF-accE Rv, pCDF-dtsR1 Fw, and pCDF-dtsR1 Rv primers. The DNA fragment encoding *coaA* was amplified from the synthetic gene using the pCDF-Acc-coaA Fw and pCDF-Acc-coaA Rv primers. The *dtsR1* fragment was inserted into pCDFDuet-1, which was double-digested with *Nde*I and *Avr*II to generate the pCDF-dtsR1 plasmid. The *accBC* fragment was inserted into pCDF-dtsR1, which was digested with *Avr*II to generate the pCDF-dtsR1-AccBC plasmid. The *accE* fragment was inserted into pCDF-dtsR1-AccBC, which was digested with *Avr*II to generate pCDF-dtsR1-AccBCE. The *coaA* fragment was inserted into pCDF-dtsR1-AccBCE, which was digested with *Avr*II to generate pCDF-Acc-CoaA.

Transformation of *E. coli*. All plasmids were used to transform *E. coli* strains via electroporation.[39]

Batch Fermentation. Precultivation of *E. coli* strains was conducted in 3 mL of LB medium containing the appropriate antibiotics in a shaker incubator at 37 °C and 200 rpm overnight. Precultured *E. coli* cells were inoculated (OD_{600} = 0.05) in 20 or 35 mL LB medium containing 0.1 M MOPS (pH 7.0, adjusted with NaOH) with appropriate antibiotics in 100 mL baffled Erlenmeyer flasks. The cultures were initially incubated at 37 °C and 200 rpm in a shaking incubator (Bio Shaker BR-43FL; Taitec, Saitama, Japan). Once the culture reached the logarithmic growth phase (OD_{600} = 0.6−0.8), 0.1 mM isopropyl β-D-thiogalactopyranoside (IPTG, Nacalai Tesque, Kyoto, Japan) and either 7.3 mM or 22 mM disodium malonate (Tokyo Chemical Industry Co., Ltd., Tokyo, Japan) were added, and the incubation temperature was changed to 20 °C with continued cultivation at 180 rpm.

To evaluate the effect of medium composition on AQ256 production, LB medium with 10 g/L glucose, LB medium with

https://doi.org/10.1021/acssynbio.5c00354
ACS Synth. Biol. 2025, 14, 3957−3966

an additional 5 g/L yeast extract (10 g/L tryptone, 10 g/L yeast extract, and 5 g/L NaCl), or M9 minimal medium (6.78 g/L Na_2HPO_4, 3.0 g/L KH_2PO_4, 0.5 g/L NaCl, 1.0 g/L NH_4Cl, 2 mM $MgSO_4$, and 0.2 mM $CaCl_2$) supplemented with 10 g/L glucose were also used for batch cultivation. These media for batch cultivation were supplemented with 0.1 M MOPS (pH 7.0) and 22 mM disodium malonate.

To investigate the effect of initial OD_{600} in batch culture, strain AQ-04 was cultivated under the conditions described above in LB medium supplemented with yeast extract and disodium malonate [10 g/L tryptone, 10 g/L yeast extract, 5 g/L NaCl, 22 mM disodium malonate, and 0.1 M MOPS (pH 7.0)]. After 6 h of induction with IPTG, the cells were harvested by centrifugation at 3500*g* for 5 min. Harvested cells were washed once with LB medium and resuspended in an appropriate volume of LB medium to prepare a concentrated cell suspension (OD_{600} = 24). This suspension was then inoculated into fresh medium at designated initial OD_{600} values of 0.5, 2.3, or 4.4. Cerulenin was added as needed to a final concentration of 50 μM.

AQ256 Extraction. A 200 μL sample of the culture medium containing *E. coli* cells was transferred to a 1.5 mL tube, frozen at − 30 °C, and subsequently thawed. Then, 200 μL of 1-butanol and 50 μL of 1 M HCl were added, and the mixture was vigorously shaken. The solution was mixed at room temperature using a microtube mixer at 2000 rpm for 10 min and then centrifuged at 10,000 rpm for 3 min. Under acidic conditions, the upper layer turned yellow, whereas the lower layer remained colorless. The upper layer was collected and mixed 1:1 (v/v) with methanol to prepare the AQ256 extract solution, which was used for analysis.

Intracellular CoA Compound Extraction. Extraction of intracellular metabolites from *E. coli* and sample preparation were performed as follows:[40] Quenching was performed by adding an equal volume of ice-cold 40% ethanol solution containing 0.8% NaCl to the collected 2 mL culture. The mixture was centrifuged at 3500 rpm, − 16 °C, for 15 min, and the cell pellet was collected. For extraction, 0.375 mL of ethanol was added, followed by vigorous vortexing and incubation at 70 °C for 15 min. The sample was then cooled on ice for 2 min, and 0.375 mL of ultrapure water was added and mixed by inversion. Subsequently, chloroform (0.5 mL) was added, and the mixture was vortexed. The mixture was centrifuged at 4000*g*, 4 °C, for 5 min, and the supernatant was collected. The collected samples were vacuum-dried using a FreeZone 2.5 Plus system (Labconco, Kansas City, MO, USA), and the dried metabolites were stored at − 80 °C. Before analysis, the metabolites were redissolved in ultrapure water at an appropriate concentration.

Analytical Methods. The concentrations of glucose and malonate in the culture medium were analyzed using high-performance liquid chromatography (HPLC) (Shimadzu Corporation, Kyoto, Japan) equipped with an Aminex HPX-87H column (7.8 mm × 300 mm, particle size 9 μm; Bio-Rad). The details of this method have been reported previously.[41]

The AQ256 standard was synthesized using ChemSpace (Riga, Latvia). The concentration of AQ256 was analyzed by HPLC using a Cosmosil 5C18-AR II column (2.0 mm × 150 mm) (Nacalai Tesque, Inc., Kyoto, Japan) with the column oven set at 40 °C. The sample injection volume was 10 μL. The mobile phase comprised acetonitrile (A) and 0.1% formic acid in water (B). The mobile phase flow rate was 0.3 mL/min. The gradient program started at 40% A for 2 min, increased to 98% A over 10 min, held for 2 min, returned to 40% A over 1 min, and maintained for 20 min. The detection was performed at 284 nm.

The concentrations of intracellular CoA compounds and ATP were analyzed by LC-MS/MS (Agilent 1260/6460; Agilent Technologies, Palo Alto, CA, USA).[42] Separation was performed using an Atlantis T3 column (2.1 mm × 150 mm, 3 μm) (Waters, Milford, MA, USA) with 5% methanol/4 mM dibutylammonium acetate (DBAA) as mobile phase A and 75% acetonitrile as mobile phase B. The flow rate was set at 0.36 mL/min. The gradient program was as follows: an initial hold at 100% A for 1 min, a decrease to 20% A over 5 min, further reduction to 0% A over 3 min, maintained for 2.5 min, returned to 100% A, and a final hold for 2.5 min. MS analysis was performed in negative mode, with the following transition conditions (m/z_parent → m/z_daughter): CoA, 766.1 → 408; acetyl-CoA, 808.1 → 408; malonyl-CoA, 852.1 → 808.1; ATP, 506.0 → 158.8.

■ ASSOCIATED CONTENT

Supporting Information

The Supporting Information is available free of charge at https://pubs.acs.org/doi/10.1021/acssynbio.5c00354.

Additional figures and lists of strains, plasmids, and primers used in this study; (Figure S1) effect of malonate concentration on AQ256 production in strain AQ-02; (Figure S2) comparison of AQ256 production in strains AQ-03 and AQ-04 with or without malonate supplementation; (Figure S3) time course of glucose concentration in the culture supernatant of strain AQ-04; (Figure S4) AQ256 production and cell growth of strain AQ-04 in M9 medium supplemented with glucose and malonate; (Figure S5) effect of cerulenin supplementation on AQ256 production in strain AQ-04; (Figure S6) time course of intracellular ATP concentration in strain AQ-04; (Figure S7) time course of CoA-related metabolites in strain AQ-04 with or without glucose supplementation; (Figure S8) ratio of intracellular to extracellular AQ256 in strain AQ-04 with or without glucose supplementation; (Figure S9) AQ256 production in strain AQ-05 overexpressing *Pl-mcat*; (Figure S10) organization and predicted functions of the *ant* biosynthetic gene cluster from *Photorhabdus laumondii* TTO1; (Table S1) list of AQ256-producing strains; (Table S2) list of plasmids; (Table S3) list of primers (PDF)

■ AUTHOR INFORMATION

Corresponding Author

Tomohisa Hasunuma − *Graduate School of Science, Technology and Innovation and Engineering Biology Research Center, Kobe University, Kobe 657-8501, Japan; RIKEN Center for Sustainable Resource Science, Yokohama, Kanagawa 230-0045, Japan;* orcid.org/0000-0002-8382-2362; Email: hasunuma@port.kobe-u.ac.jp

Authors

Takatoshi Suematsu − *Graduate School of Science, Technology and Innovation, Kobe University, Kobe 657-8501, Japan; Konica Minolta, Inc., Hachioji, Tokyo 192-8505, Japan*

https://doi.org/10.1021/acssynbio.5c00354
ACS Synth. Biol. 2025, 14, 3957−3966

Manami Takama − *Graduate School of Science, Technology and Innovation, Kobe University, Kobe 657-8501, Japan; Konica Minolta, Inc., Hachioji, Tokyo 192-8505, Japan*
Itsuki Tomita − *Graduate School of Science, Technology and Innovation, Kobe University, Kobe 657-8501, Japan*
Shumpei Asamizu − *Engineering Biology Research Center, Kobe University, Kobe 657-8501, Japan;* orcid.org/0000-0002-7178-5410
Takahiro Bamba − *Engineering Biology Research Center, Kobe University, Kobe 657-8501, Japan;* orcid.org/0009-0009-2679-2900

Complete contact information is available at: https://pubs.acs.org/10.1021/acssynbio.5c00354

Author Contributions

T.S., S.A., T.B., and T.H. designed the experiments. T.S., M.T., and I.T. performed the experiments. All authors discussed the results. T.S., S.A., T.B., and T.H. wrote the manuscript. S.A., T.B., and T.H. supervised all aspects of the study.

Notes

The authors declare no competing financial interest.

■ ACKNOWLEDGMENTS

This research was supported by the Program for Forming Japan's Peak Research Universities (J-PEAKS) from JSPS and the GteX Program Japan from Japan Science and Technology Agency (JST, grant no. JPMJGX23B4). We also thank Dr. Noboru Yumoto (Kobe University) and Mr. Takanobu Yoshida (Kobe University) for providing technical advice.

■ REFERENCES

(1) Caro, Y.; Anamale, L.; Fouillaud, M.; Laurent, P.; Petit, T.; Dufosse, L. Natural Hydroxyanthraquinoid Pigments as Potent Food Grade Colorants: An Overview. *Nat. Prod. Bioprospect.* **2012**, *2*, 174−193.
(2) Zhang, X.; Good, I.; Laursen, R. Characterization of Dyestuffs in Ancient Textiles from Xinjiang. *J. Archaeol. Sci.* **2008**, *35*, 1095−1103.
(3) Xu, K.; Wang, P.; Wang, L.; Liu, C.; Xu, S.; Cheng, Y.; Wang, Y.; Li, Q.; Lei, H. Quinone Derivatives from the Genus Rubia and Their Bioactivities. *Chem. Biodiversity* **2014**, *11*, 341−363.
(4) Wang, D.; Wang, X. H.; Yu, X.; Cao, F.; Cai, X.; Chen, P.; Li, M.; Feng, Y.; Li, H.; Wang, X. Pharmacokinetics of Anthraquinones from Medicinal Plants. *Front. Pharmacol.* **2021**, *12*, No. 638993.
(5) Fouillaud, M.; Venkatachalam, M.; Girard-Valenciennes, E.; Caro, Y.; Dufossé, L. Anthraquinones and Derivatives from Marine-Derived Fungi: Structural Diversity and Selected Biological Activities. *Mar. Drugs* **2016**, *14*, No. 64.
(6) Raghuveer, D.; Pai, V. V.; Murali, T. S.; Nayak, R. Exploring Anthraquinones as Antibacterial and Antifungal Agents. *ChemistrySelect* **2023**, *8*, No. e202204537.
(7) Malik, E. M.; Müller, C. E. Anthraquinones As Pharmacological Tools and Drugs. *Med. Res. Rev.* **2016**, *36*, 705−748.
(8) Shamim, G.; Ranjan, S. K.; Pandey, D. M.; Ramani, R. Biochemistry and Biosynthesis of Insect Pigments. *Eur. J. Entomol.* **2014**, *111*, 149−164.
(9) Singh, R.; Geetanjali; Chauhan, S. M. S. 9,10-Anthraquinones and Other Biologically Active Compounds from the Genus Rubia. *Chem. Biodiversity* **2004**, *1*, 1241−1264.
(10) Mund, N. K.; Čellárová, E. Recent Advances in the Identification of Biosynthetic Genes and Gene Clusters of the Polyketide-Derived Pathways for Anthraquinone Biosynthesis and Biotechnological Applications. *Biotechnol. Adv.* **2023**, *63*, No. 108104.
(11) Han, Y.-S.; van der Heijden, R.; Lefeber, A. W. M.; Erkelens, C.; Verpoorte, R. Biosynthesis of Anthraquinones in Cell Cultures of *Cinchona 'Robusta'* Proceeds via the Methylerythritol 4-Phosphate Pathway. *Phytochemistry* **2002**, *59* (1), 45−55.
(12) Shen, B. Polyketide Biosynthesis beyond the Type I, II and III Polyketide Synthase Paradigms. *Curr. Opin. Chem. Biol.* **2003**, *7*, 285−295.
(13) Wang, J.; Zhang, R.; Chen, X.; Sun, X.; Yan, Y.; Shen, X.; Yuan, Q. Biosynthesis of Aromatic Polyketides in Microorganisms Using Type II Polyketide Synthases. *Microb. Cell Fact.* **2020**, *19*, 110.
(14) Zhang, Q.; Wang, X.; Zeng, W.; Xu, S.; Li, D.; Yu, S.; Zhou, J. De Novo Biosynthesis of Carminic Acid in *Saccharomyces cerevisiae*. *Metab. Eng.* **2023**, *76*, 50−62.
(15) Yang, D.; Eun, H.; Prabowo, C. P. S. Metabolic Engineering and Synthetic Biology Approaches for the Heterologous Production of Aromatic Polyketides. *Int. J. Mol. Sci.* **2023**, *24*, No. 8923.
(16) Yang, D.; Jang, W. D.; Lee, S. Y. Production of Carminic Acid by Metabolically Engineered *Escherichia coli*. *J. Am. Chem. Soc.* **2021**, *143*, 5364−5377.
(17) Stevens, D. C.; Conway, K. R.; Pearce, N.; Villegas-Peñaranda, L. R.; Garza, A. G.; Boddy, C. N. Alternative Sigma Factor Over-Expression Enables Heterologous Expression of a Type II Polyketide Biosynthetic Pathway in *Escherichia coli*. *PLoS One* **2013**, *8*, No. e64858.
(18) Liu, X.; Hua, K.; Liu, D.; Wu, Z. L.; Wang, Y.; Zhang, H.; Deng, Z.; Pfeifer, B. A.; Jiang, M. Heterologous Biosynthesis of Type II Polyketide Products Using *E. coli*. *ACS Chem. Biol.* **2020**, *15*, 1177−1183.
(19) Cummings, M.; Peters, A. D.; Whitehead, G. F. S.; Menon, B. R. K.; Micklefield, J.; Webb, S. J.; Takano, E. Assembling a Plug-and-Play Production Line for Combinatorial Biosynthesis of Aromatic Polyketides in *Escherichia coli*. *PLoS Biol.* **2019**, *17*, No. e3000347.
(20) Sohn, Y. J.; Kim, H. T.; Jo, S. Y.; Song, H. M.; Baritugo, K. A.; Pyo, J.; Choi, J. il; Joo, J. C.; Park, S. J. Recent Advances in Systems Metabolic Engineering Strategies for the Production of Biopolymers. *Biotechnol. Bioprocess Eng.* **2020**, *25*, 848−861.
(21) Zhang, W.; Li, Y.; Tang, Y. Engineered Biosynthesis of Bacterial Aromatic Polyketides in *Escherichia coli*. *Proc. Natl. Acad. Sci. U.S.A.* **2008**, *105*, 20683−20688.
(22) Bräuer, A.; Zhou, Q.; Grammbitter, G. L. C.; Schmalhofer, M.; Rühl, M.; Kaila, V. R. I.; Bode, H. B.; Groll, M. Structural Snapshots of the Minimal PKS System Responsible for Octaketide Biosynthesis. *Nat. Chem.* **2020**, *12*, 755−763.
(23) Bennett, B. D.; Kimball, E. H.; Gao, M.; Osterhout, R.; Van Dien, S. J.; Rabinowitz, J. D. Absolute Metabolite Concentrations and Implied Enzyme Active Site Occupancy in *Escherichia coli*. *Nat. Chem. Biol.* **2009**, *5*, 593−599.
(24) Davis, M. S.; Solbiati, J.; Cronan, J. E. Overproduction of Acetyl-CoA Carboxylase Activity Increases the Rate of Fatty Acid Biosynthesis in *Escherichia coli*. *J. Biol. Chem.* **2000**, *275*, 28593−28598.
(25) Zha, W.; Rubin-Pitel, S. B.; Shao, Z.; Zhao, H. Improving Cellular Malonyl-CoA Level in *Escherichia coli* via Metabolic Engineering. *Metab. Eng.* **2009**, *11*, 192−198.
(26) Leonard, E.; Lim, K. H.; Saw, P. N.; Koffas, M. A. G. Engineering Central Metabolic Pathways for High-Level Flavonoid Production in *Escherichia coli*. *Appl. Environ. Microbiol.* **2007**, *73*, 3877−3886.
(27) Kaku, M.; Ishidaira, M.; Satoh, S.; Ozaki, M.; Kohari, D.; Chohnan, S. Fatty Acid Production by Enhanced Malonyl-CoA Supply in *Escherichia coli*. *Curr. Microbiol.* **2022**, *79*, 275.
(28) Satoh, S.; Ozaki, M.; Matsumoto, S.; Nabatame, T.; Kaku, M.; Shudo, T.; Asayama, M.; Chohnan, S. Enhancement of Fatty Acid Biosynthesis by Exogenous Acetyl-CoA Carboxylase and Pantothenate Kinase in *Escherichia coli*. *Biotechnol. Lett.* **2020**, *42*, 2595−2605.
(29) Liang, B.; Sun, G.; Wang, Z.; Xiao, J.; Yang, J. Production of 3-Hydroxypropionate Using a Novel Malonyl-CoA-Mediated Biosynthetic Pathway in Genetically Engineered *Escherichia coli* Strain. *Green Chem.* **2019**, *21*, 6103−6115.
(30) Moteallehi-Ardakani, M. H.; Asad, S.; Marashi, S. A.; Moghaddasi, A.; Zarparvar, P. Engineering a Novel Metabolic

Pathway for Improving Cellular Malonyl-CoA Levels in *Escherichia coli*. *Mol. Biotechnol.* **2023**, *65*, 1508−1517.
(31) Wu, J.; Zhou, T.; Du, G.; Zhou, J.; Chen, J. Modular Optimization of Heterologous Pathways for de Novo Synthesis of (2S)-Naringenin in *Escherichia coli*. *PLoS One* **2014**, *9*, No. e101492.
(32) Ogata, Y.; Chohnan, S. Prokaryotic Type III Pantothenate Kinase Enhances Coenzyme A Biosynthesis in *Escherichia coli*. *J. Gen. Appl. Microbiol.* **2015**, *61*, 266−269.
(33) Livieri, A. L.; Navone, L.; Marcellin, E.; Gramajo, H.; Rodriguez, E. A Novel Multidomain Acyl-CoA Carboxylase in *Saccharopolyspora erythraea* Provides Malonyl-CoA for de Novo Fatty Acid Biosynthesis. *Sci. Rep.* **2019**, *9*, 43223.
(34) Omura, S. The Antibiotic Cerulenin, a Novel Tool for Biochemistry as an Inhibitor of Fatty Acid Synthesis. *Bacteriol. Rev.* **1976**, *40*, 681−697.
(35) Chen, H.; Kim, H. U.; Weng, H.; Browse, J. Malonyl-CoA Synthetase, Encoded by ACYL ACTIVATING ENZYME13, Is Essential for Growth and Development of *Arabidopsis*. *Plant Cell* **2011**, *23*, 2247−2262.
(36) Wright, M.; Kaur, M.; Thompson, L. K.; Cox, G. A Historical Perspective on the Multifunctional Outer Membrane Channel Protein TolC in Escherichia coli. npj Antimicrob. *Resist.* **2025**, *3*, 6.
(37) Sezonov, G.; Joseleau-Petit, D.; D'Ari, R. Escherichia coli Physiology in Luria-Bertani Broth. *J. Bacteriol.* **2007**, *189*, 8746−8749.
(38) Youssef, S. M.; Abdella, E. M. M.; Al-Elwany, O. A.; Alshallash, K. S.; Alharbi, K.; Ibrahim, M. T. S.; Tawfik, M. M.; Abu-Elsaoud, A. M.; Elkelish, A. Integrative Application of Foliar Yeast Extract and Gibberellic Acid Improves Morpho-Physiological Responses and Nutrient Uptake of *Solidago virgaurea* Plant in Alkaline Soil. *Life* **2022**, *12*, No. 1405.
(39) Green, M.; Sambrook, J. *Molecular Cloning: A Laboratory Manual*; 4th ed.; Cold Spring Harbor Laboratory Press: New York, 2012.
(40) Takenaka, M.; Yoshida, T.; Hori, Y.; Bamba, T.; Mochizuki, M.; Vavricka, C. J.; Hattori, T.; Hayakawa, Y.; Hasunuma, T.; Kondo, A. An Ion-Pair Free LC-MS/MS Method for Quantitative Metabolite Profiling of Microbial Bioproduction Systems. *Talanta* **2021**, *222*, No. 121625.
(41) Bamba, T.; Yukawa, T.; Guirimand, G.; Inokuma, K.; Sasaki, K.; Hasunuma, T.; Kondo, A. Production of 1,2,4-Butanetriol from Xylose by *Saccharomyces cerevisiae* through Fe Metabolic Engineering. *Metab. Eng.* **2019**, *56*, 17−27.
(42) Deja, S.; Fletcher, J. A.; Kim, C. W.; Kucejova, B.; Fu, X.; Mizerska, M.; Villegas, M.; Pudelko-Malik, N.; Browder, N.; Inigo-Vollmer, M.; Menezes, C. J.; Mishra, P.; Berglund, E. D.; Browning, J. D.; Thyfault, J. P.; Young, J. D.; Horton, J. D.; Burgess, S. C. Hepatic Malonyl-CoA Synthesis Restrains Gluconeogenesis by Suppressing Fat Oxidation, Pyruvate Carboxylation, and Amino Acid Availability. *Cell Metab.* **2024**, *36* (5), 1088−1104.e12.

https://doi.org/10.1021/acssynbio.5c00354
ACS Synth. Biol. 2025, 14, 3957−3966